Journal of Inorganic Biochemistry 276 (2026) 113154

Contents lists available at ScienceDirect

Journal of Inorganic Biochemistry

journal homepage: www.elsevier.com/locate/jinorgbio

Dehalogenation activity of a miniaturized peroxidase: substrate dependent functional switch☆

Maria De Fenza [a,*], Linda Leone [a], Matilde Tancredi [a], Edelberto Oscar Niola [a], Ornella Maglio [a,b], Gerardino D'Errico [a], Flavia Nastri [a], Daniele D'Alonzo [a], Angela Lombardi [a,*]

[a] Department of Chemical Sciences, University of Napoli Federico II, Via Cintia, 80126 Napoli, Italy,
[b] Institute of Biostructures and Bioimaging, National Research Council, Napoli, Italy

ARTICLE INFO

Keywords:
Artificial peroxidase
Halophenols
EPR spectroscopy
Phenoxyl radicals
Kinetic studies
Competitive inhibition

ABSTRACT

Natural peroxidases use 4-halophenols either as substrates in oxidative chemistry or as inhibitors. Herein, we demonstrated that Fe-mimochrome VI*a (Fe-MC6*a), a miniaturized heme-enzyme, is a versatile catalyst as it integrates both these features. We previously reported that Fe-MC6*a catalyzes the chemo- and regio-selective oxidation of 4-halophenols, providing either dehalogenation or oligomerization products, depending on the nature of the halogen atom. In particular, 4-chlorophenol (4-CP) and 4-fluorophenol (4-FP) selectively led to dehalogenation and oligomerization products, respectively. Herein, spin-trapping studies and EPR analysis confirm the ability of Fe-MC6*a into processing halophenols as substrates and provide mechanistic hypothesis for the chemo-divergent reaction outcome. Further, in multiple substrate competition assays, 4-halophenols act as competitive inhibitors of Fe-MC6*a-catalyzed dehalogenation of 2,4,6-trichlorophenol (TCP). Nonetheless, the catalyst retains appreciable turnover in such complex substrate mixtures. Taken together, the combination of substrate-specific selectivity and resilience to the total inhibition position Fe-MC6*a as a promising bioremediation catalyst for simultaneous halophenol detoxification in wastewater-treatment applications.

1. Introduction

The design of metalloenzymes that combine promiscuous catalytic potential with the ability to perform highly selective transformations remains one of the foremost challenges in biocatalysis [1,2]. Metalloenzymes have been conceived by Nature to perform chemical transformations with remarkable efficiency and selectivity. The occurrence of appropriate protein scaffolds results into modulation of the redox properties of metal cofactors by direct metal ion coordination and/or by second coordination sphere interactions [3]. However, the intricate network of non-covalent interactions required for their function often results into a narrow substrate specificity, which limits a broad application as biocatalysts. Inspired by Nature, efforts have been focused on the design of artificial metalloenzymes (ArMs). They are engineered either to reproduce the reactivity of natural metalloenzymes or to enable "new-to-nature" transformations, while offering enhanced functional properties such as higher catalytic efficiency, broader substrate scope, and improved reaction selectivity [4–8]. Over the last decades, several strategies have been developed, including de novo design [9,10], protein redesign [6,11], directed evolution [12,13] or supramolecular assembly [14]. The class of miniaturized metalloenzymes, named "Mimochromes" (MCs), fits within this context. Featuring minimal protein scaffolds, composed of two alpha-helical peptide chains covalently linked to a deuteroporphyrin unit, MCs represent simple but effective heme-enzyme models [15]. The latest member of the series, MC6*a, has emerged as a robust [16], efficient [17] and highly versatile catalyst. MC6*a is able to integrate in a single molecule the activities of metalloenzymes with diverse catalytic properties, such as peroxidases [18], peroxygenases [19] or hydrogenases [20–22], depending on the metal ion inserted into the porphyrin. Applications of MCs span from the synthesis of added value chemicals [23] to the design of a fully artificial electron chain [7], from the assembly of biohybrid materials [24,25] to their application as biosensors [26] or as components for lateral flow immunoassays [27].

Recently, we have further expanded the catalytic potential of the iron-containing MC6*a (Fe-MC6*a, Fig. 1a) exploring its role in the

☆ This article is part of a Special issue entitled: 'Metal-Binding Peptides' published in Journal of Inorganic Biochemistry.

* Corresponding authors.
E-mail addresses: maria.defenza@unina.it (M. De Fenza), alombard@unina.it (A. Lombardi).

https://doi.org/10.1016/j.jinorgbio.2025.113154
Received 1 August 2025; Received in revised form 31 October 2025; Accepted 17 November 2025
Available online 19 November 2025

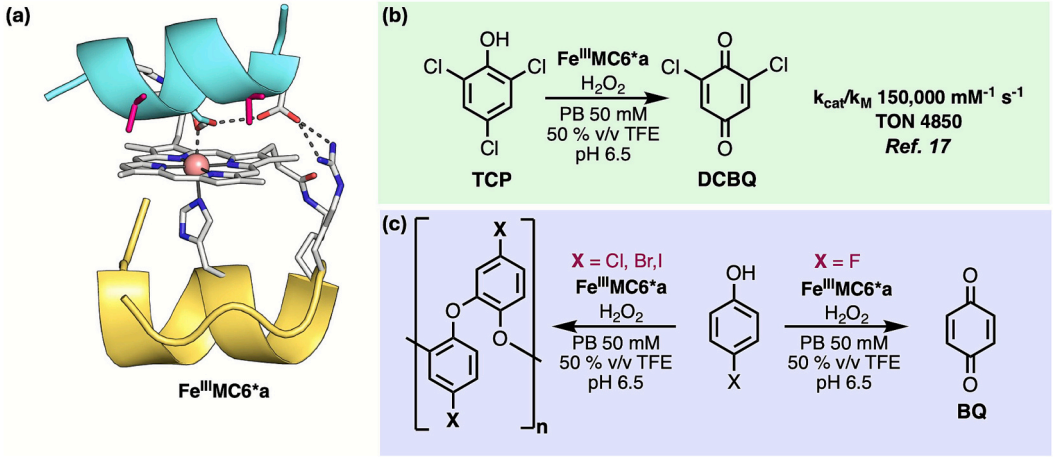

Fig. 1. (a) Molecular model of Fe-MC6*a. (b) Oxidative dechlorination of 2,4,6-trichlorophenol (TCP) catalyzed by Fe-MC6*a. (c) Halogen-dependent chemo-divergent 4-halophenol oxidation catalyzed by Fe-MC6*a.

H_2O_2-mediated oxidation of a broad range of mono-, di-, tri- and penta-halophenols [17,28]. Halophenols represent highly valuable substrates for oxidative catalysis. On one hand, they are key components of numerous bioactive molecules [29], therefore, their selective conversion into synthetic intermediates results attractive for pharmaceutical applications. On the other hand, halophenols are one of the most widespread classes of environmental contaminants [30] due to their use as pesticides, herbicides, fungicides and dyes [31]. Consequently, efforts are still required to identify new and efficient technologies for their transformation. The use of oxidoreductases, such as peroxidases or phenoloxidases, which catalyze the conversion of these pollutants into less toxic molecules, represents nowadays one of the most promising approaches [30].

Our previous studies on halophenol oxidation have established the ability of Fe-MC6*a to outperform natural and artificial biocatalysts [31–34]. Kinetic studies of the Fe-MC6*a-catalyzed oxidation of 2,4,6-trichlorophenol (TCP) revealed that the dechlorination reaction yielding 2,6-dichloro-1,4-benzoquinone (DCBQ, Fig. 1b) proceeds with a catalytic efficiency surpassing that of any other natural or artificial metalloenzyme reported to date [17]. In addition, when investigating the oxidation of 4-halogenated phenols (4-XPs, X = F, Cl, Br, I), Fe-MC6*a exhibited even more peculiar enzymatic properties, as it promotes highly selective, substrate-dependent chemo-divergent transformations (Fig. 1c), leading to oxidative dehalogenation and formation of benzoquinone (BQ) for 4-FP or C—O bond forming oligomerization products in the case of the others 4-XPs. [28]

This finding highlights the broad substrate scope of Fe-MC6*a toward 4-XPs respect to peroxidases. Indeed, depending on the accessibility of the active site, peroxidases (including horseradish peroxidase, HRP [32]; chloroperoxidase, CPO [33,34]; microperoxidase, MP8 [35]) use 4-halophenols either for oxidative dehalogenation [35] or for oligo- and polymerization, albeit without any significant chemo- and regio-selectivity control [32,34]. Conversely, in the case of dehaloperoxidases A and B (DHP A and DHP B), 4-XPs act as inhibitors, competitively interfering with their oxidative activities [36,37].

The observed catalytic versatility of Fe-MC6*a may represent an added value in view of its potential application for the treatment of tainted media, which may contain different mixtures of the above-mentioned pollutants. In this context, we have herein further analyzed the reactivity of Fe-MC6*a toward 4-halophenols, to shed light on the reaction mechanism responsible for the observed chemo-selectivity. Next, we focused on catalyst promiscuity by shifting from single-substrate screening to multiple-substrate competition assays, analyzing the effects of 4-XPs on the oxidative dehalogenation of TCP. This study revealed that, besides their role as substrates, 4-XPs behave as inhibitors significantly interfering with TCP dehalogenation. However, the catalyst retains detectable activity even in substrate mixtures, thus demonstrating its efficacy to function in different conditions.

2. Materials and methods

2.1. Materials

All solvents were supplied by Romil (Cambridge, UK). All reagents including 2,2,2-trifluoroethanol (TFE), 4-chlorophenol, 4-fluorophenol, 4-bromophenol, 4-iodophenol, 2,4,6-trichlorophenol, hydrogen peroxide (H_2O_2) solution (50 % (*v*/v)), phosphate salts (mono- and di-basic), 2-methylpyrroline, diisopropylphosphite, 1,4-benzoquinone (BQ), boron trifluoride diethyl etherate, sodium tungstate, potassium ferricyanide, methyl phenyl sulfone (MPS) and chlorobenzene (CB) were purchased from Merck (Merck KGaA, Darmstadt, Germany). Fe-MC6*a was synthesized, purified and characterized as previously described [38]. The Fe-MC6*a concentration was determined by UV–Vis spectroscopy using $\varepsilon = 1.17 * 10^5\ M^{-1}\ cm^{-1}$ in H_2O 0.1 % TFA (v/v) (λ_{max} = 387 nm).

2.2. Equipment and methods

UV–Vis spectra were recorded on a Cary Varian 60 Probe UV spectrophotometer equipped with a temperature controller (Varian, Palo Alto, CA, USA). Quartz cuvettes with a path length of 1.0 cm were used for the measurements. The wavelength scans were performed from 200 to 800 nm, with a 600 nm min^{-1} scan speed. All data were blank subtracted. The data analysis was performed using Origin Pro, version 9.0 (Origin Lab Corporation, Northampton, MA, USA). NMR spectra were acquired using Bruker Avance 600 or 400 MHz spectrometers (Karlsruhe, Germany). All NMR experiments were carried out at 298 K. All spectra were processed with MestreNova (version 14.2.2). EPR spectra were acquired using the X-band spectrometer Elexys E-500 super-high sensitivity probehead (Bruker, Rheinstetten, Germany), and processed with Xepr (version 1.1 Beta). GC–MS analysis was performed on a Shimadzu GCMS-QP2010 SE system equipped with an EI-MS source, a quadrupole array as an MS analyzer (Shimadzu Corporation, Kyoto, Japan) and a Shimadzu GC–MS solution Workstation (version 4.20) for data processing. A Restek Rxi-5Sil-MS column was used, with helium being selected as the carrier gas. A linear gradient from 50 °C to 300 °C with a rate of 24 °C min^{-1} was used. The mass spectra were recorded in an *m/z* range between 50 and 450. The molar absorptivity (ε) was determined using UV–vis spectroscopy.

2.3. Phenoxyl radical detection

DIPPMPO synthesis: the spin-trapping agent, 5-diisopropoxy-phosphoryl-5-methyl-1-pyrroline-*N*-oxide (DIPPMPO), was prepared as already reported [39]. 2-Methylpyrroline (2.0 g, 2.3 mL, 1.0 eq.) was added to a round-bottom flask containing diisopropylphosphite (4.4 g, 4.4 mL, 1.1 eq.) at room temperature (RT). Freshly distilled boron trifluoride diethyl etherate (0.30 mL, 0.1 eq.) was slowly added to the reaction mixture. The reaction was stirred in the dark for 72 h. Then, further 0.4 eq. of diisopropylphosphite were added to bring the reaction to completion. When 2-methylpyrroline was no longer detectable by TLC, 2 M HCl was added until pH 3 and the aqueous phase was washed twice with methyl *t*-butyl ether (MTBE). After adjustment of the aqueous phase pH to 9–10 by addition of NaOH in pellets, this was extracted 4 times with CH_2Cl_2. The organic phase was then dried on Na_2SO_4 and 5.75 g of an orange oil were obtained after solvent evaporation. ^{1}H NMR and ^{31}P NMR spectra acquisition confirmed the identity of diisopropyl (2-methyl-2-pyrrolidinyl)phosphonate (96 % yield), as they were found in agreement with the literature data [39]. Diisopropyl (2-methyl-2-pyrrolidinyl)phosphonate (2.0 g, 1.0 eq.) was added to sodium tungstate (0.094 g, 0.04 eq.), dissolved in 5 mL of distilled water. To the solution cooled down to 0 °C, hydrogen peroxide 30 % (1.9 mL, 2.2 eq.) was added dropwise. The pale-yellow reaction mixture was stirred at 0 °C until the colour darkened, then it was stirred at 10 °C for several hours, and the progress of the oxidation was monitored by TLC. When the oxidation stopped, a new quantity of H_2O_2 (0.5 eq.) was added to oxidize the pyrrolidine moiety. When the reaction was complete, the reaction product was extracted with CH_2Cl_2. The collected organic phases were dried with Na_2SO_4 and the solvent was removed under reduced pressure. The crude nitrone (2.0 g) was purified by direct-phase chromatography (silica gel, 60 g, DCM:EtOH 80:20). The collected fractions were concentrated by solvent evaporation and stored at −20 °C. ^{1}H NMR and ^{31}P NMR spectra in CD_2Cl_2 confirmed the identity of DIPPMPO. The collected spectra are fully in agreement with literature data [40].

*Spin-trapping experiments with Fe-MC6*a*: time-dependent UV–Vis spectra of 4-FP and 4-CP, (0.250 mM) were acquired every minute (overall for 10 min) upon H_2O_2 addition (0.250 mM) to a solution of Fe-MC6*a (6.25×10^{-4} mM) and DIPPMPO (12.5 mM) in 50 mM sodium phosphate (pH 6.5) with 50 % TFE (v/v).

Spin-trapping experiments with $K_3[Fe(CN)_6]$: time-dependent UV–Vis spectra of 4-FP and 4-CP (0.250 mM) in presence of DIPPMPO (12.5 mM) in 50 mM sodium phosphate (pH 6.5) with 50 % TFE (v/v) were acquired every minute (for 30 min) upon addition of $K_3[Fe(CN)_6]$ (0.350 mM).

2.4. EPR measurements

*Fe-MC6*a-catalyzed 4-halophenol oxidation*: a solution of H_2O_2 (final concentration: 0.250 mM) was added in one portion at room temperature to a stirring solution of 4-CP or 4-FP (final concentration: 0.250 mM) and Fe-MC6*a (final concentration: 6.25×10^{-4} mM) in 50 mM sodium phosphate (pH 6.5) with TFE (1/1 v/v). The reaction was carried out in an overall reaction volume of 0.6 mL. The reaction was left while stirring for 10 min at RT, then 20 μL were inserted into a glass capillary and immediately flame sealed. The capillary was coaxially collocated into a typical 4 mm quartz sample tube. Spectra were recorded at RT. The instrument parameters were as follows: sweep width, 400 G; resolution, 1024 points; sweep time, 20.60 s; modulation amplitude, 1.0 G; microwave power, 20.09. The *g* value and spin concentration were obtained using an internal standard, Mn^{2+}-doped MgO, prepared as previously described [41], a weighted amount of which, sealed in a capillary, was placed in the quartz tube co-axial with the capillary containing the sample.

Uncatalyzed 4-halophenol oxidation: a solution of $K_3[Fe(CN)_6]$ (final concentration: 0.350 mM) was added in one portion at RT to a stirring solution of 4-CP or 4-FP (final concentration: 0.250 mM) in 50 mM sodium phosphate (pH 6.5) with TFE (1/1 v/v). The reaction was carried out in an overall reaction volume of 0.6 mL. The reaction was left while stirring for 10 min at RT. An aliquot (20 μL) of the reaction mixture was placed in flame-sealed glass capillary that was coaxially collocated into a 4 mm quartz sample tube. Spectra were recorded at the same conditions used for the catalyzed oxidation samples.

2.5. Inhibition studies

Initial rate dependence from pH: solutions of TCP (0.250 mM) and Fe-MC6*a (6.25×10^{-5} mM) in the appropriate buffer (pH 4.5–8.5; 50 mM acetate or phosphate buffer) containing 50 % (v/v) TFE were treated with a solution of H_2O_2 (0.250 mM). Progress curves were recorded by monitoring the formation of DCBQ at 272 nm. The initial rates (v_o) were determined from the slope of the tangent to the absorbance-time curve at the earliest stage of the reactions.

UV–Vis studies: time-dependent UV–Vis spectra of TCP (0.250 mM) in the absence or in the presence of 4-FP, 4-CP, 4-BP and 4-IP (0.500 mM) were acquired every min (overall for 10 min) upon H_2O_2 addition (0.250 mM) to a solution of Fe-MC6*a ($6.25*10^{-5}$ mM) in 50 mM sodium phosphate (pH 6.5) with 50 % TFE (v/v).

GC–MS analysis: a solution of H_2O_2 (final concentration 2.5 mM) was added in one portion at RT to a stirring solution of TCP (2.5 or 5.0 mM), 4-halophenol (2.5 or 5.0 mM), MPS (2.5 mM) or CB (2.5 mM) and Fe-MC6*a (3.10×10^{-3} mM or 6.25×10^{-4} mM) in 50 mM sodium phosphate (pH 6.5) with TFE (1/1 v/v). The reaction was carried out in an overall reaction volume of 0.5 mL. Aliquots (50 μL) were withdrawn before ($t = 0$) and after ($t = 30$ min) H_2O_2 addition and transferred to 0.5 mL Eppendorf tubes. The reaction mixtures were quenched by the addition of a H_2O 0.1 % TFA (v/v) solution (50 μL) and extracted with dichloromethane (100 μL). Organic layers were dried (Na_2SO_4), centrifuged at 4000 rpm and the supernatants were injected.

TON determination: the turnover number (TON) was determined by GC–MS analysis of the reaction, measuring the conversion degree based on the maximal substrate consumption. Following the procedure reported in the previous paragraph, total ion current (TIC) chromatograms were acquired. The peak areas corresponding to TCP and MPS (or CB) were integrated for all reaction times. When monitoring the oxidation of TCP in the presence of 4-IP, MPS was replaced by CB as the internal standard due to the overlapping retention times between 4-IP and MPS. The conversion degree was calculated using the following equation (Eq. 1):

$$Conversion\ (\%) = 100*\frac{\left(\frac{A_{TCP}}{A_{I.Std.}}\right)_0 - \left(\frac{A_{TCP}}{A_{I.Std.}}\right)_{30}}{\left(\frac{A_{TCP}}{A_{I.Std.}}\right)_0} \quad (1)$$

where A_{TCP} and $A_{I.Std.}$ are the peak areas of the substrate and the internal standard, respectively, in the GC–MS TIC chromatogram. The subscript 0 indicates the trace acquired prior to H_2O_2 addition, while the subscript 30 is the specific time during the reaction. Based on the conversion degree, the TON value was calculated as the ratio between the number of converted substrate molecules and the number of catalyst molecules. The mean TON values along with the corresponding standard errors are reported in Table S1.

2.6. Kinetic analysis

BQ molar extinction coefficient determination: two BQ stock solutions were prepared dissolving 108.0 mg of solid powder in 10.0 mL of phosphate buffer solution 100 mM (pH 6.5) with 50 % of TFE (final BQ concentration: 100 mM). Starting from these stock solutions, two intermediate diluted solutions (10 mM) were prepared (5.0 mL final volume). Ten diluted solutions (1.5–3.0 mM) were then prepared from the last stock solutions (final volume: 1.0 mL) and used to obtain the ε value

at 301 nm. The UV-Vis absorption spectra and the plot of the absorbance at 301 nm as a function of BQ concentration are reported in Fig. S3. The experimental data were fitted to Lambert-Beer's law, giving a $\varepsilon_{301} = 289 \pm 6\ M^{-1}\ cm^{-1}$.

4-FP kinetic parameters determination: K_m values for 4-FP and H_2O_2 were measured keeping constant one of the two substrate concentrations, while varying the other one and vice versa. Progress curves of the reaction were monitored at $\lambda = 301$ nm, with an average time of 0.1 s. Fe-MC6*a concentration in all experiments was fixed at $6.25*10^{-4}$ mM in phosphate buffer (50 mM, pH 6.5) with 50 % TFE (v/v). For the determination of K_m (H_2O_2), 4-FP concentration was fixed at 400 μM, while H_2O_2 concentration was varied from 0 to 200 mM. For the determination of K_m (4-FP), H_2O_2 concentration was fixed at 250 mM, while 4-FP concentration was varied from 0 to 500 μM. Initial rate (v_0) values were plotted as a function of both substrates concentration and data points were fitted according to the two-substrates Michaelis and Menten equation below (Eq. 2), using Origin Pro 9.0 software:

$$v_0 = \frac{[E_0]}{\frac{1}{k_{cat}} + \frac{K_{m(a)}}{k_{cat}[A]} + \frac{K_{m(b)}}{k_{cat}[B]}} \quad (2)$$

where $[E_0]$ is the initial concentration of the enzyme, k_{cat} is the catalytic constant, $K_{m(a)}$ and $K_{m(b)}$ are the Michaelis–Menten constants for 4-FP and H_2O_2 respectively, and [A] and [B] are the concentrations of 4-FP and H_2O_2, respectively. From data fitting, K_m and k_{cat} values were calculated.

TCP kinetic parameters determination: to evaluate enzyme activity, the formation of DCBQ was followed at $\lambda = 272$ nm ($\varepsilon = 15.8*10^3\ M^{-1}\ cm^{-1}$). Fe-MC6*a concentration in all experiments was fixed at $6.25*10^{-5}$ mM in phosphate buffer (50 mM, pH 6.5) with 50 % TFE (v/v). For K_m(TCP) determination, H_2O_2 concentration was fixed at 250 mM, 4-FP concentration was fixed at 250 μM or at 500 μM, while TCP concentration was varied from 0 to 1 mM. The initial rate (v_0, mM s^{-1}) values were plotted as a function of the substrate concentrations, and the data points were fitted according to a one-substrate Michaelis–Menten equation (Eq. 3) using Origin Pro 9.0 software. From data fitting, K_m and V_{max} values were determined.

$$v_0 = \frac{V_{max}[TCP]}{K_m + [TCP]} \quad (3)$$

3. Results and discussion

3.1. Fe-MC6*a oxidative dehalogenation of para-halophenols: insights into the reaction mechanism

We have previously reported [17,28] that the general mechanism for the Fe-MC6*a catalyzed oxidative dehalogenation of halophenols proceeds via a two-step, single electron oxidation pathway (see Scheme 1). H_2O_2 conversion of the Fe-MC6*a resting ferric state gives rise to the oxoferrylporphyrin radical cation intermediate [(Fe(IV)]=O)por$^{\cdot+}$], similar to peroxidase compound I (Cpd I), which promotes the one-

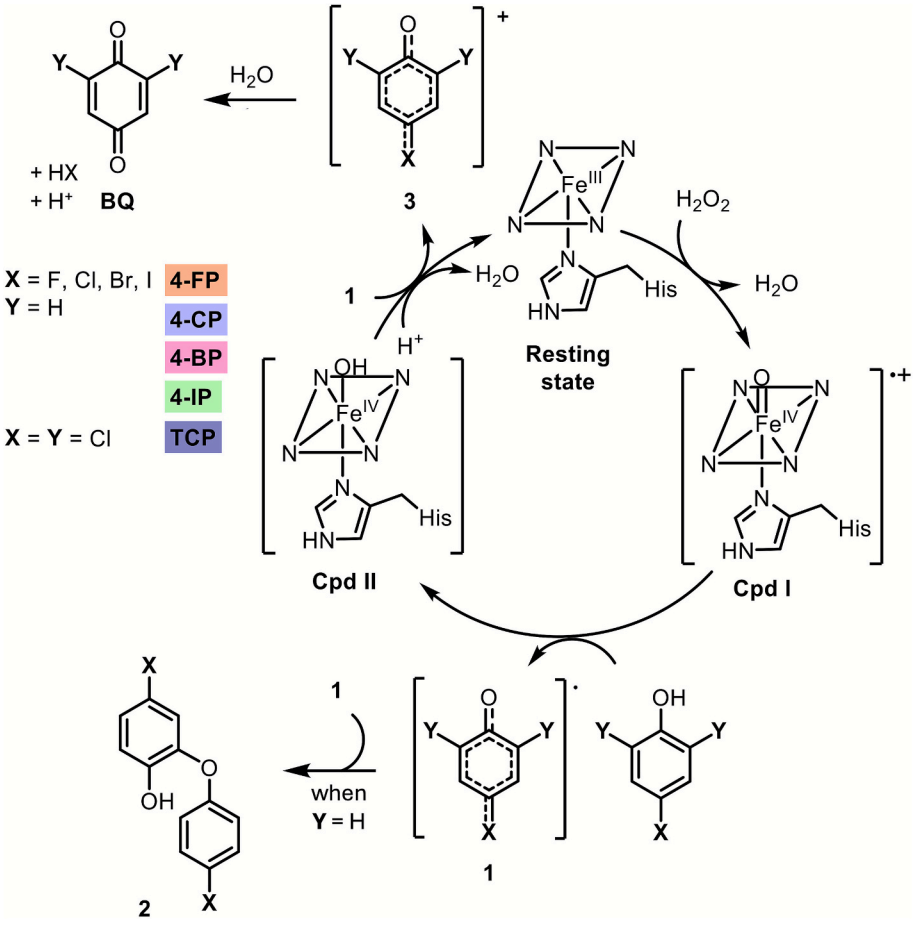

Scheme 1. Fe-MC6*a -catalyzed oxidation of halophenols: catalytic cycle.

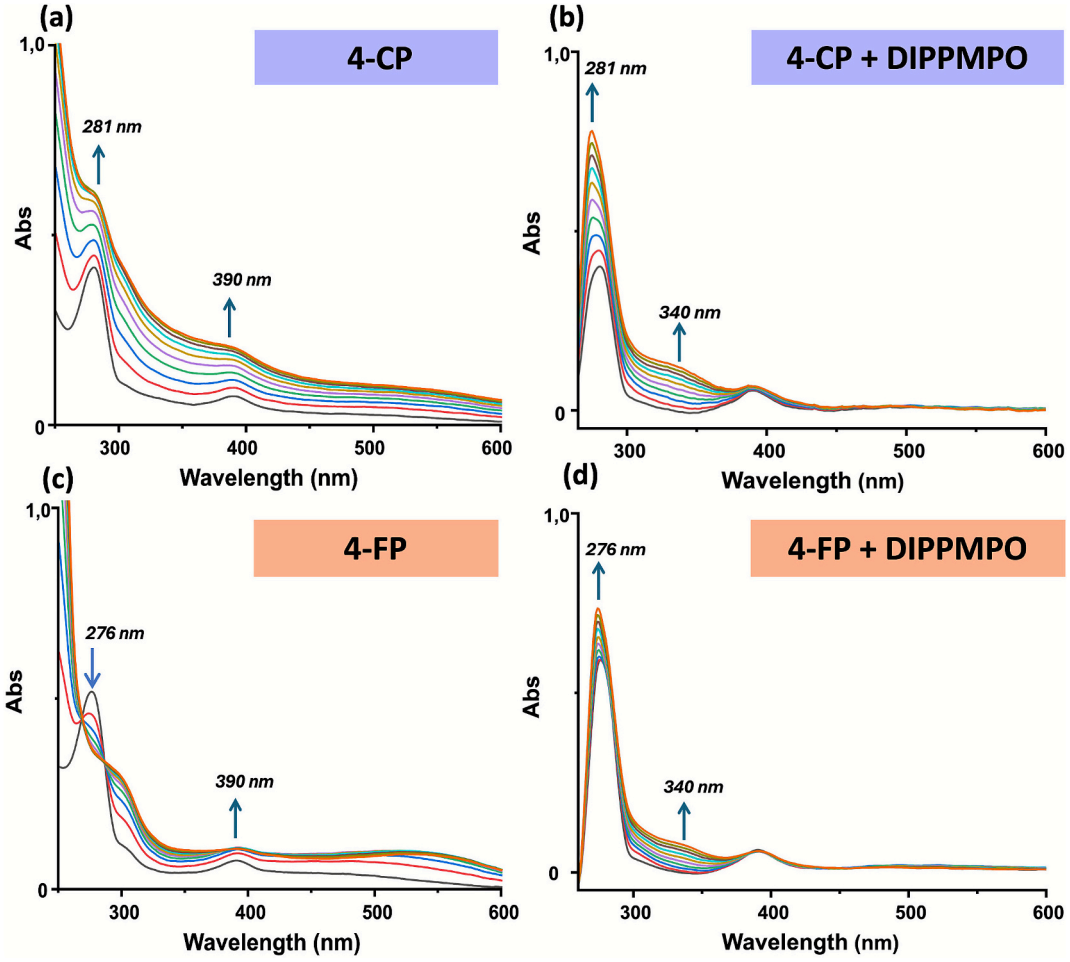

Fig. 2. (a),(c) Time-dependent UV–Vis spectra (acquired over 10 min) of 4-CP (0.250 mM, (a)) or 4-FP (0.250 mM, (c)) in the presence of Fe-MC6*a (6.25×10^{-4} mM) in 50 mM sodium phosphate (pH 6.5) with 50 % TFE (v/v) upon H_2O_2 addition (0.250 mM). Black line, $t = 0$ min; orange line, 10 min; spectra taken every 1 min are reported in different colours. (b),(d) Time-dependent UV–Vis spectra (acquired over 10 min) of 4-CP (0.250 mM, (b)) or 4-FP (0.250 mM, (d)) in the presence of Fe-MC6*a (6.25×10^{-4} mM), 50 eq. of DIPPMPO (12.5 mM) in 50 mM sodium phosphate (pH 6.5) with 50 % TFE (v/v) upon H_2O_2 addition (0.250 mM). Black line, t = 0 min; orange line, 10 min; spectra taken every 1 min are reported in different colours.

electron oxidation of the substrate to the phenoxyl radical intermediate **1**. Further one-electron oxidation of the phenoxyl radical **1** yields a positively charged dienone species **3**. This dienone can be converted into BQ upon reaction with a water molecule, which replaces the halide ion as leaving group. Conversely, self-coupling reactions among radicals **1** are expected to provide dimer **2**, which subsequently leads to the formation of oligomers.

Based on this catalytic cycle, the key for the origin of the observed substrate-dependent chemo-divergent oxidative dehalogenation of 4-XPs would be a different accumulation of radical **1**, depending on the halide nature. Indeed, accumulation of radical **1** is expected to favour the formation of self-coupling products, while a higher concentration of **3** would drive toward the selective conversion of 4-XP into BQ.

To test this hypothesis, we detected and quantified the radical species produced during the conversion of 4-FP and 4-CP using spin-trapping experiments in combination with UV–Vis and EPR spectroscopy. To this end, the 5-diisopropoxy-phosphoryl-5-methyl-1-pyrroline-*N*-oxide, namely DIPPMPO, a phosphorous-containing nitrone spin-trapping agent, was selected for its ability to form radical adducts with extended half-lives [42].

Oxidation of 4-FP or 4-CP was performed in the experimental conditions previously reported [28] (0.250 mM substrates, Fe-MC6*a 6.25 $\times 10^{-4}$ mM for both substrates, H_2O_2 0.250 mM in phosphate buffer 50 mM/TFE (50 % v/v) at pH 6.5), either in the absence or in the presence of the spin-trapping agent (DIPPMPO 12.5 mM).

UV–Vis analysis of the reaction mixtures carried out in the presence

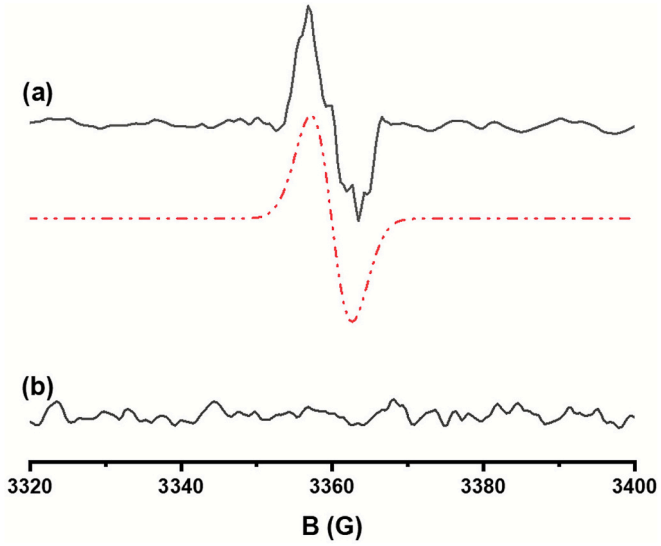

Fig. 3. EPR spectra of 4-CP (0.250 mM, (a)) or 4-FP (0.250 mM, (b)) in the presence of Fe-MC6*a (6.25×10^{-4} mM) in 50 mM sodium phosphate (pH 6.5) with 50 % TFE (v/v), acquired after 10 min upon H_2O_2 addition (0.250 mM). Black line, experimental spectra; red line, spectrum fitted to a gaussian line shape.

of DIPPMPO (Fig. 2b and 2d) shows different profiles respect to the reaction carried out in the absence of DIPPMPO (Fig. 2a and 2c). When the spin-trapping agent is present, a time-dependent increase of an absorption band at 340 nm can be observed for both 4-FP and 4-CP. Such band can be assigned to the formation of a covalent adduct between the 4-halophenoxyl radical and DIPPMPO. Indeed, the same band is observed when 4-CP and 4-FP were treated with DIPPMPO and hexacyanoferrate (III), used as a one-electron oxidizing agent (Fig. S1a-b) [39]. These results suggest that, for both substrates, formation of organic radicals is involved in the reaction mechanism.

EPR measurements were subsequently used to quantify the radical species formed during the reactions (Fig. 3). The EPR spectrum of the reaction mixture for 4-CP oxidation catalyzed by Fe-MC6*a, acquired after 10 min incubation upon H_2O_2 addition, displayed a signal at a *g* value of 2.0040 (Fig. 3a). The singlet is typically associated to organic radicals, in which the unpaired electron is stabilized by delocalization in an aromatic system, and the *g* value indicates significant contribution of heteroatoms. No coupling with hydrogen atoms was detectable, possibly due to the presence of several radical species with slightly different signals. Indeed, this seems to be supported by the relatively broad gaussian line shape. The spin concentration was estimated to be around 10 μM. Notably, no signal of organic radicals was detected in the EPR spectrum of the same reaction when using 4-FP as the substrate (Fig. 3b). When the same reaction was carried out with hexacyanoferrate(III) as the one-electron oxidizing agent, identical EPR spectra were obtained for either 4-CP or 4-FP (Fig. S2), characterized by a barely detectable signal at the same *g* value. All these spectroscopic findings suggest that the Fe-MC6*a catalyzed oxidative dehalogenation of both 4-CP and 4-FP involves the formation of 4-halophenoxyl radicals, as previously hypothesized (see Scheme 1), which, in the case of 4-CP, accumulates, thus resulting in an EPR detectable signal. Accumulation of the 4-chlorophenoxyl radical would in turn allow its oxidative coupling, thus driving toward the formation of oligomeric products and supporting the observed substrate-dependent chemo-selectivity.

3.2. An in-depth analysis of Fe-MC6*a-catalyzed oxidative dehalogenation: effects of para-halophenols on TCP oxidation

Given that Fe-MC6*a can convert both 4- and 2,4,6-halogenated phenols, it is interesting to explore whether such a small peptide-based peroxidase is able to discriminate between 4-XPs and TCP, as similarly reported for natural dehaloperoxidases. [36,37] Indeed, the oxidative dehalogenation of TCP catalyzed by both DHP A and B is significantly inhibited by all 4-XPs, acting as competitive inhibitors. [37] This behavior has been attributed to the unique substrate-binding properties of DHPs. When TCP is the only substrate, it can bind either at an internal or at an external site. [43] Conversely, in bi-component assays, 4-XPs preferentially occupy the internal binding site, thereby forcing TCP to bind at the external site. [36,37,44]

The effect of pH on the oxidation of TCP catalyzed by Fe-MC6*a was first evaluated. In previous studies [17], Fe-MC6*a-catalyzed TCP oxidation was assayed at pH 6.5, the optimal pH value for peroxidase activity toward ABTS oxidation. [16] To address whether the protonation state of the substrate may have a role in the reaction outcome, we investigated the influence of pH by monitoring the initial rates of the oxidation reactions at three different pH values (4.5, 6.5 and 8.5). The v_0 value at pH 6.5 (0.23 μM/s) was much higher than those at pH 4.5 (0.032 μM/s) and at pH 8.5 (0.031 μM/s). The results confirmed that the maximum catalytic activity of Fe-MC6*a is still reached at pH 6.5, regardless of the substrate protonation state.

We then investigated the effect of 4-XPs on the Fe-MC6*a-catalyzed TCP oxidation. Fig. 4 reports the time-dependent UV–Vis spectra for TCP conversion in the absence or in the presence of 4-XPs, at a 4-XP:TCP ratio of 2:1. In the absence of 4-XPs, TCP was readily converted to DCBQ as clearly indicated by the drop in the intensity of the substrate band (310 nm) and the appearance of the product band at 272 nm (Fig. 4a). On the opposite, in the presence of all 4-XPs, TCP conversion proceeded to a lesser extent, as no significant decrease of the 310 nm substrate band was observed (Fig. 4b-e), and only a smaller increase in the intensity of the band at 272 nm was detectable over time.

For a quantitative analysis of the inhibitory effect of each 4-XP on TCP dehalogenation, the reaction was also followed by GC–MS. Consistent with our earlier findings, [17] in the absence of 4-XPs and after 30 min from H_2O_2 addition, almost complete TCP conversion was observed (TON: 3551 ± 258, Fig. 5 and Table S1). On the opposite, a remarkable drop in the TON values was observed when TCP oxidation was carried out in the presence of 4-FP (TON: 496 ± 42), 4-CP (TON: 384 ± 48) and 4-BP (TON: 357 ± 49) (see Table S1 in ESI). In the case of 4-IP, a slightly minor decrease in the TON value (TON: 677 ± 57) was detected (Fig. 5 and Table S1). The inhibitory effect of TCP on 4-XP dehalogenation was also evaluated. Because of the lower TON values of 4-XPs (4-FP: 503 ± 10; 4-CP: 325 ± 22; 4-BP: 235 ± 10; 4-IP: 208 ±

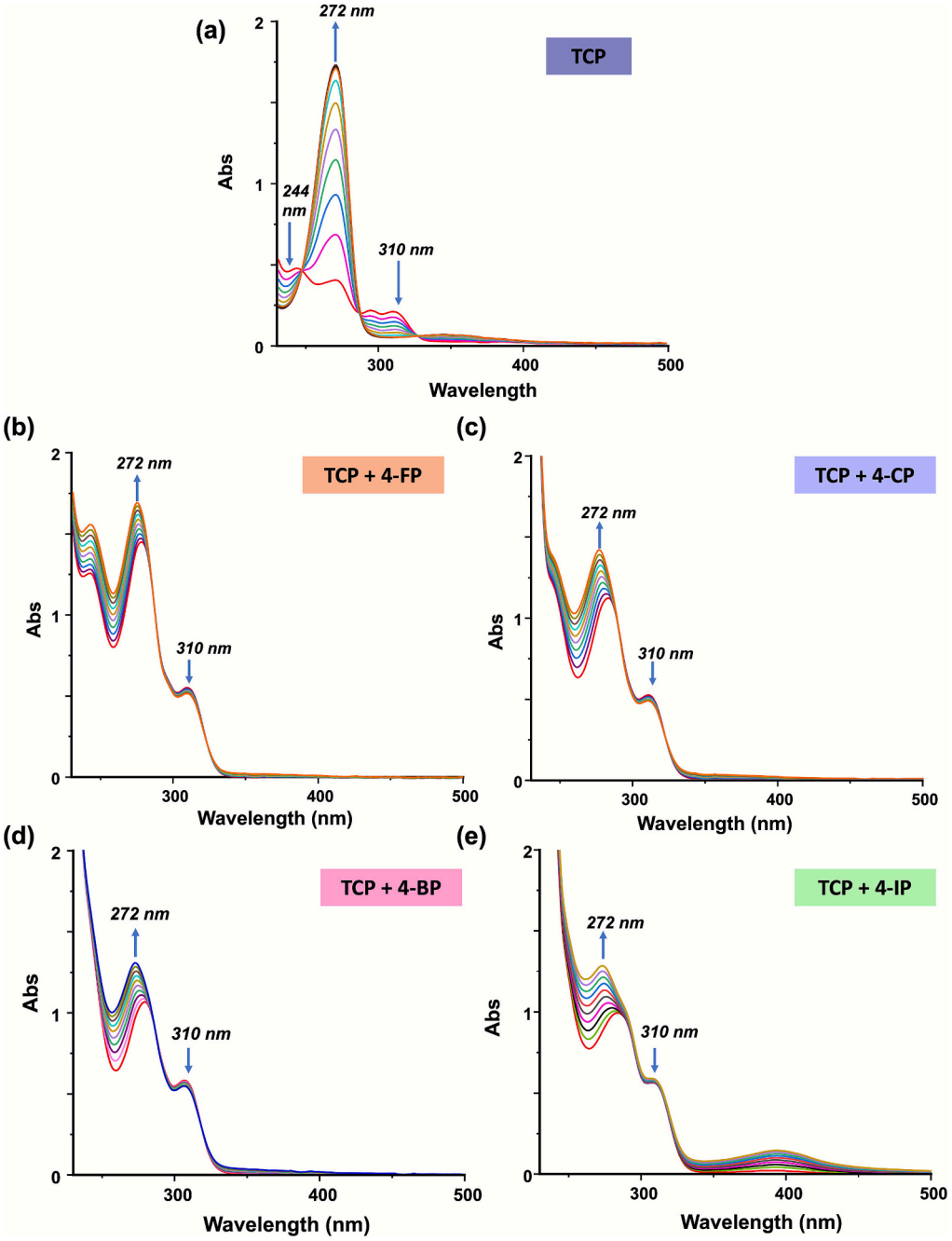

Fig. 4. Time-dependent UV–Vis spectra of Fe-MC6*a oxidation of TCP in the absence (a) or in the presence of 4-XPs ((b) 4-FP, (c) 4-CP, (d) 4-BP and (e) 4-IP). *General conditions:* [Fe-MC6*a] = 6.25×10^{-5} mM; [TCP] = 0.250 mM; [4-XP] = 0.500 mM; [H_2O_2] = 0.250 mM; 50 mM phosphate buffer, pH 6.5 with 50 % (v/v) TFE. In all cases the spectrum before H_2O_2 addition is marked as red. Spectra were collected each 60 s at 25 °C.

30) [28] than TCP (3551 ± 258) [17], a lower substrate-to-catalyst ratio was used (Table S1), compared to the previously used conditions (see Fig. 5), to accurately evaluate 4-XP consumption. Under these new conditions, the formation of markedly heterogenous reaction mixtures, due to the presence of insoluble oligomerization products, prevented the acquisition of reliable measurements in the case of 4-CP, 4-BP and 4-IP. In the case of 4-FP, we found that its TON value (503 ± 10; Table S1) [28] was only minimally reduced by the presence of TCP (16% inhibition; TON = 423 ± 33, entry 4, Table S1). Inverting the 4-FP:TCP ratio from 2:1 to 1:2, the 4-FP turnover was more markedly affected (40 % inhibition; TON = 300 ± 16; entry 5, Table S1). Conversely, in both experiments the TCP turnover was more significantly while identically reduced (85–86 % inhibition; Table S1, entries 4–5). Taken together, UV–Vis and GC–MS data show that each 4-XP substantially reduces the TON values of the Fe-MC6*a-catalyzed TCP oxidation, independently from the nature of the halogen atom. Further, TCP also reduces the 4-FP turnovers, although to a lesser extent. All these findings suggest that 4-FP and TCP are competitive substrates; nevertheless, 4-FP acts as a stronger inhibitor of TCP dehalogenation, even when present in a lower 4-FP:TCP ratio.

To get further insights into the role of 4-XPs as inhibitors of TCP oxidation, the kinetic parameters in the presence of 4-FP, selected as a representative inhibitor of the series, were measured. Michaelis-Menten analysis of the initial reaction rate versus TCP concentration, in the absence or in the presence of two different 4-FP concentrations (250 and 500 μM), is reported in Fig. 6 and Table 1.

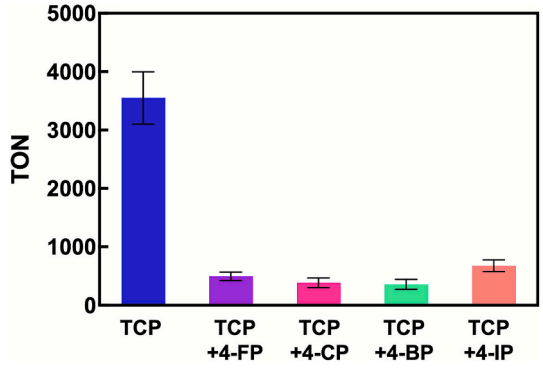

Fig. 5. TON values of the Fe-MC6*a-catalyzed oxidation of TCP in the absence or in the presence of 4-XPs. *General conditions:* [Fe-MC6*a] = 6.25*10^{-4} mM; [TCP] = 2.5 mM; [4-XP] = 5.0 mM; [H_2O_2] = 2.5 mM; 50 mM phosphate buffer, pH 6.5 with 50 % (v/v) TFE. MPS was used as internal standard ([MPS] = 2.5 mM). In the case of 4-IP, CB was used as internal standard ([CB] = 2.5 mM).

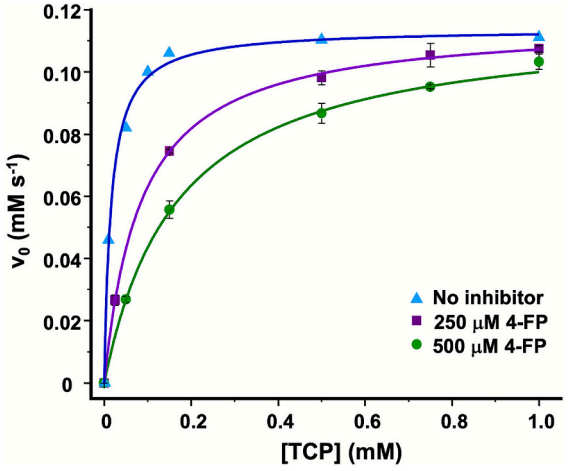

Fig. 6. Michaelis-Menten analysis showing the initial rate versus TCP concentration, in the absence of the inhibitor (blue curve) or in the presence of two different 4-FP concentrations (violet: 0.250 mM; green: 0.500 mM). *General conditions:* Fe-MC6*a (6.25*10^{-5} mM), H_2O_2 (250 mM) in 50 mM phosphate buffer pH 6.5/TFE (1:1 v/v).

Table 1
Kinetic parameters of Fe-MC6*a in the oxidative dehalogenation of TCP in the absence or in the presence of 4-FP.

Entry	Inhibitor	V_{max} (μM/s)	K_m (μM)
1	**None**	113 ± 2	16 ± 1
2	**4-FP (250 μM)**	120 ± 8	85 ± 10
3	**4-FP (500 μM)**	117 ± 8	167 ± 5

The relative effect of 4-FP on the reaction kinetic is evident. Addition of 4-FP resulted in an increase in the K_m(TCP) values, as the concentration of this substrate increases. In the absence of 4-FP, the best fit of the curve (Fig. 6, blue line, Table 1) gave the values V_{max} = 113 μM s^{-1} and K_m = 16 ± 1 μM. In the presence of different concentrations of 4-FP, kinetic measurements showed an increase in the K_m values, being 85 ± 10 μM and 167 ± 5 μM at 250 μM and 500 μM 4-FP, respectively (entries 2 and 3).

Lineweaver-Burk plot of the data (see Fig. S4) supports that Fe-MC6*a catalysis of TCP in the presence of 4-FP fits the kinetic model of reversible enzyme inhibition. Indeed, in the presence of two different concentrations of 4-FP, straight lines that intersect *y*-axis at a same point were obtained, thus indicating that V_{max} of the reaction remained essentially unchanged (see Fig. S4 and Table 1). From the straight lines intersection of *x*-axis, the apparent K_m were found variable with respect to concentration of 4-FP, and consistent with the values reported in Table 1. All these results suggest that in this condition 4-FP acts as a competitive inhibitor of the TCP oxidation reaction catalyzed by Fe-MC6*a. According to Ascenzi *et al.* [45] as 4-FP determines only the increase of the K_m value for the TCP substrate, the inhibition dissociation constant (K_i) of the enzyme-inhibitor (EI) complex can be calculated by the following equation: $K_m^{app} = K_m (1 + [I]/K_i)$, in which K_m^{app} is the apparent Michaelis constant for TCP in the presence of constant inhibitor concentration [I] and K_i is the inhibition dissociation constant of the EI complex. This calculation for 4-FP gives a value of $K_i^{4\text{-FP}} = 52 \pm 1$ μM.

Further, as 4-FP is also a substrate for Fe-MC6*a, the kinetic data obtained on TCP conversion in the presence of 4-FP can be interpreted in terms of competition between the two substrates for the same enzyme [46]. This competition in turns depends on the relative affinities of the two substrates for the active site, and their concentration used in the assay. In a mixture of TCP and 4-FP, each substrate may act as a competitive inhibitor of the other. However, the effect of TCP on the kinetic parameters of 4-FP cannot be easily measured as the bands at 245 and 301 nm, characteristic of BQ as 4-FP oxidative dehalogenation product, overlap with TCP bands. Thus, a quantitative kinetic analysis on the inhibitor behavior was performed only on 4-FP.

To this end, the kinetic parameters for the H_2O_2-dependent 4-FP dehalogenation catalyzed by Fe-MC6*a (Fig. 7) were measured and compared with those previously determined for the Fe-MC6*a-catalyzed TCP oxidation [17] (Table 2).

Inspection of Table 2 shows that Fe-MC6*a converts 4-FP and TCP with similar turnover frequency (k_{cat}). The Michaelis–Menten constant value for 4-FP (K_m: 52 ± 5 μM) was 3-fold higher than K_m for TCP oxidation (K_m: 16 ± 2 μM), thus affording a catalytic efficiency (k_{cat}/K_m^{halo}) toward 4-FP about 3-fold lower than TCP. These results demonstrate the specificity of Fe-MC6*a toward TCP. [47] This specificity may account for the observed catalyst performances in the mixed substrate assays. Indeed, the addition of a two-fold amount of 4-XPs does not completely inhibit Fe-MC6*a catalyzed oxidative TCP dehalogenation, as the measured TON value for TCP conversion in the mixture lowers to a value comparable to those observed for the isolated 4-XPs [28].

To evaluate whether the redox potential of the substrates may contribute to the reaction outcome, the reduction potentials (E_{red}°) of phenol/phenoxyl and phenolate/phenoxyl couples were analyzed. At pH 7, the reported E_{red}° values for 4-XPs are: 4-FP, +0.93 V; 4-CP, +0.94 V; 4-BP, +0.96 V; 4-IP, +0.96 V. [48] The calculated E_{red}° for TCP is +0.88 V. [49] Based on these values, TCP represents the thermodynamically most favorable substrate for oxidation to the corresponding phenoxyl radical. Even though E_{red}° values of halophenols have been correlated with k_{cat} of certain peroxidases, [50] in our case the k_{cat} values for TCP and 4-FP are closely comparable, despite their different redox potentials. This suggests that the catalytic activity is not primarily governed by the stability of the phenoxyl radicals, while other factors

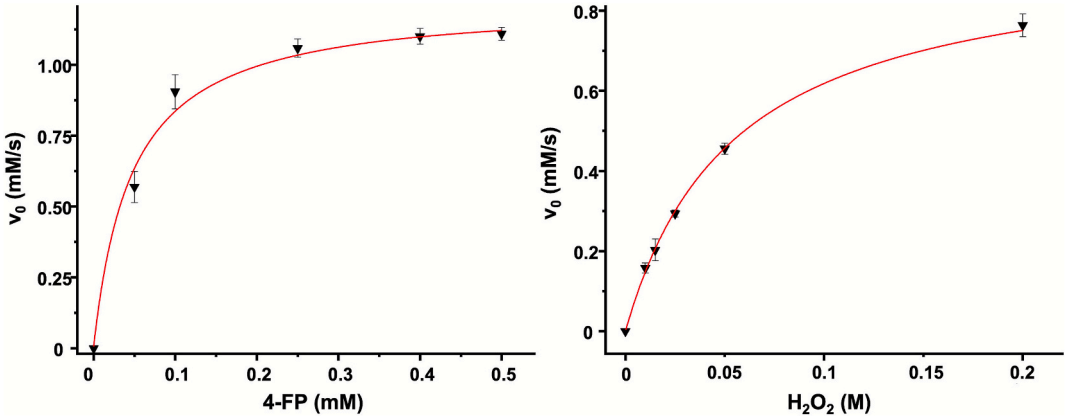

Fig. 7. 4-FP oxidative dehalogenation activity of Fe-MC6*a. (a) Initial rate dependence toward 4-FP concentration. *Reaction conditions*: Fe-MC6*a ($6.25*10^{-4}$ mM), H_2O_2 (250 mM) in 50 mM phosphate buffer pH 6.5/TFE (1:1 v/v). (b) Initial rate dependence toward H_2O_2 concentration. *Reaction conditions*: Fe-MC6*a ($6.25*10^{-4}$ mM), 4-FP (0.400 mM) in 50 mM phosphate buffer pH 6.5/TFE (1:1 v/v).

Table 2
Kinetic parameters of Fe-MC6*a in the oxidative dehalogenation of 4-FP and TCP.

Entry	Substrate	K_m^{halo} (μM)	K_m^{H2O2} (10^3 μM)	k_{cat} (s^{-1})	k_{cat}/K_m^{halo} (10^2 μM^{-1} s^{-1})
1	**4-FP**	52 ± 5	67.9 ± 7	2100 ± 20	0.405
2	**TCP**[a]	16 ± 2	120 ± 10	2400 ± 80	1.50

[a] The steady-state kinetic parameters for TCP are taken from [17].

may play a role to more significantly determining the rate-limiting step of the catalytic cycle.

4. Conclusions

In this work we have highlighted the versatility of Fe-MC6*a as catalyst in the oxidative dehalogenation of differently substituted halophenols. In the conversion of 4-XPs, Fe-MC6*a is able to process similar substrates following different pathways. In the presence of the catalyst, 4-halophenoxyl radicals differently accumulate in the reaction mixture depending on the halogen nature. This finding explains why 4-CP oxidation predominantly provides radical-assisted oligomerization products, while the reaction with 4-FP selectively leads to the corresponding defluorination product (BQ). The crucial role of Fe-MC6*a is confirmed by control experiments with hexacyanoferrate(III), which in both cases produce only a barely detectable EPR signal attributable to 4-halophenoxyl radicals. Further computational studies will help to better elucidate the observed chemo-divergence.

In addition, in multiple substrate competition assays, all 4-XPs act as inhibitors of the Fe-MC6*a-catalyzed TCP oxidation. Despite the marked decrease in the catalytic performance (regarding both the TON value and the kinetic parameters), the catalyst retains measurable activity even in the presence of these substrate mixtures. These distinctive properties highlight the peculiar catalytic versatility of the MC6*a scaffold and suggest potential applications of Fe-MC6*a in bioremediation processes, where the simultaneous degradation of multiple halophenol contaminants in wastewater is often required.

CRediT authorship contribution statement

Maria De Fenza: Writing – review & editing, Writing – original draft, Visualization, Investigation, Formal analysis. **Linda Leone:** Writing – original draft, Visualization, Investigation, Formal analysis. **Matilde Tancredi:** Visualization, Investigation. **Edelberto Oscar Niola:** Investigation. **Ornella Maglio:** Investigation, Formal analysis. **Gerardino D'Errico:** Writing – review & editing, Formal analysis. **Flavia Nastri:** Writing – review & editing, Validation, Supervision, Conceptualization. **Daniele D'Alonzo:** Writing – original draft, Investigation, Conceptualization. **Angela Lombardi:** Writing – review & editing, Validation, Supervision, Project administration, Funding acquisition, Conceptualization.

Declaration of competing interest

The authors declare that they have no known competing financial interests or personal relationships that could have appeared to influence the work reported in this paper.

Acknowledgements

We wish to thank Prof. Vincenzo Pavone for his never-ending interest in this study and for numerous fruitful discussions. M.D.F. is grateful to the Italian MUR for being granted a research fellow position (PONR&I 2014–2020, CUP E65F21003010003). The work herein described was supported by Italian MUR, PRIN 2020, Project SEA-WAVE 2020BKK3W9, [CUP E69J22001140005]. The authors finally acknowledge the Italian MUR program "Dipartimenti di Eccellenza 2023-2027" for the project arCHIMede [CUP E63C22003710006].

Appendix A. Supplementary data

Supplementary data to this article can be found online at https://doi.org/10.1016/j.jinorgbio.2025.113154.

Data availability

Data will be made available on request.

References

[1] R.B. Leveson-Gower, C. Mayer, G. Roelfes, The importance of catalytic promiscuity for enzyme design and evolution, Nat Rev Chem 3 (2019) 687–705, https://doi.org/10.1038/s41570-019-0143-x.
[2] A. Lombardi, F. Pirro, O. Maglio, M. Chino, W.F. DeGrado, De novo Design of Four-Helix Bundle Metalloproteins: one scaffold, diverse Reactivities, Acc. Chem. Res. 52 (2019) 1148–1159, https://doi.org/10.1021/acs.accounts.8b00674.
[3] W.J. Jeong, J. Lee, H. Eom, W.J. Song, A specific guide for metalloenzyme designers: introduction and evolution of metal-coordination spheres embedded in

protein environments, Acc. Chem. Res. 56 (2023) 2416–2425, https://doi.org/10.1021/acs.accounts.3c00336.
[4] L. Leone, M. De Fenza, A. Esposito, O. Maglio, F. Nastri, A. Lombardi, Peptides and metal ions: a successful marriage for developing artificial metalloproteins, J. Pept. Sci. 30 (2024) e3606, https://doi.org/10.1002/psc.3606.
[5] I. Morita, T.R. Ward, Recent advances in the design and optimization of artificial metalloenzymes, Curr. Opin. Chem. Biol. 81 (2024) 102508, https://doi.org/10.1016/j.cbpa.2024.102508.
[6] C. Van Stappen, Y. Deng, Y. Liu, H. Heidari, J.-X. Wang, Y. Zhou, A.P. Ledray, Y. Lu, Designing artificial Metalloenzymes by tuning of the environment beyond the primary coordination sphere, Chem. Rev. 122 (2022) 11974–12045, https://doi.org/10.1021/acs.chemrev.2c00106.
[7] M. Chino, L.F. Di Costanzo, L. Leone, S. La Gatta, A. Famulari, M. Chiesa, A. Lombardi, V. Pavone, Designed Rubredoxin miniature in a fully artificial electron chain triggered by visible light, Nat. Commun. 14 (2023) 2368, https://doi.org/10.1038/s41467-023-37941-8.
[8] S. La Gatta, L. Leone, O. Maglio, M. De Fenza, F. Nastri, V. Pavone, M. Chino, A. Lombardi, Unravelling the structure of the tetrahedral metal-binding site in METP3 through an experimental and computational approach, Molecules 26 (2021) 5221, https://doi.org/10.3390/molecules26175221.
[9] M.J. Chalkley, S.I. Mann, W.F. DeGrado, De novo metalloprotein design, Nat. Rev. Chem. 6 (2021) 31–50, https://doi.org/10.1038/s41570-021-00339-5.
[10] Y.-W. Lin, Functional metalloenzymes based on myoglobin and neuroglobin that exploit covalent interactions, J. Inorg. Biochem. 257 (2024) 112595, https://doi.org/10.1016/j.jinorgbio.2024.112595.
[11] T. Hayashi, Y. Sano, A. Onoda, Generation of new artificial metalloproteins by cofactor modification of native hemoproteins, Isr. J. Chem. 55 (2015) 76–84, https://doi.org/10.1002/ijch.201400123.
[12] K. Chen, F.H. Arnold, Engineering new catalytic activities in enzymes, Nat. Catal. 3 (2020) 203–213, https://doi.org/10.1038/s41929-019-0385-5.
[13] R.S. Molina, G. Rix, A.A. Mengiste, B. Álvarez, D. Seo, H. Chen, J.E. Hurtado, Q. Zhang, J.D. García-García, Z.J. Heins, P.J. Almhjell, F.H. Arnold, A.S. Khalil, A. D. Hanson, J.E. Dueber, D.V. Schaffer, F. Chen, S. Kim, L.Á. Fernández, M. D. Shoulders, C.C. Liu, In vivo hypermutation and continuous evolution, Nat. Rev. Methods Primers 2 (2022) 36, https://doi.org/10.1038/s43586-022-00119-5.
[14] B. Maity, M. Taher, S. Mazumdar, T. Ueno, Artificial metalloenzymes based on protein assembly, Coord. Chem. Rev. 469 (2022) 214593, https://doi.org/10.1016/j.ccr.2022.214593.
[15] F. Nastri, D. D'Alonzo, L. Leone, G. Zambrano, V. Pavone, A. Lombardi, Engineering metalloprotein functions in designed and native scaffolds, Trends Biochem. Sci. 44 (2019) 1022–1040, https://doi.org/10.1016/j.tibs.2019.06.006.
[16] G. Caserta, M. Chino, V. Firpo, G. Zambrano, L. Leone, D. D'Alonzo, F. Nastri, O. Maglio, V. Pavone, A. Lombardi, Enhancement of peroxidase activity in artificial Mimochrome VI catalysts through rational design, ChemBioChem 19 (2018) 1823–1826, https://doi.org/10.1002/cbic.201800200.
[17] G. Zambrano, A. Sekretareva, D. D'Alonzo, L. Leone, V. Pavone, A. Lombardi, F. Nastri, Oxidative dehalogenation of trichlorophenol catalyzed by a promiscuous artificial heme-enzyme, RSC Adv. 12 (2022) 12947–12956, https://doi.org/10.1039/D2RA00811D.
[18] M. Chino, S. La Gatta, L. Leone, M. De Fenza, A. Lombardi, V. Pavone, O. Maglio, Dye decolorization by a miniaturized peroxidase fe-mimochromeVI*a, Int. J. Mol. Sci. 24 (2023) 11070, https://doi.org/10.3390/ijms241311070.
[19] L. Leone, D. D'Alonzo, V. Balland, G. Zambrano, M. Chino, F. Nastri, O. Maglio, V. Pavone, A. Lombardi, Mn-mimochrome VI*a: an artificial metalloenzyme with peroxygenase activity, Front. Chem. 6 (2018) 590, https://doi.org/10.3389/fchem.2018.00590.
[20] V. Firpo, J.M. Le, V. Pavone, A. Lombardi, K.L. Bren, Hydrogen evolution from water catalyzed by cobalt-mimochrome VI*a, a synthetic mini-protein, Chem. Sci. 9 (2018) 8582–8589, https://doi.org/10.1039/C8SC01948G.
[21] J.M. Le, G. Alachouzos, M. Chino, A.J. Frontier, A. Lombardi, K.L. Bren, Tuning mechanism through buffer dependence of hydrogen evolution catalyzed by a cobalt mini-enzyme, Biochemistry 59 (2020) 1289–1297, https://doi.org/10.1021/acs.biochem.0c00060.
[22] A.A. Salamatian, J.L. Alvarez-Hernandez, K.B. Ramesh, L. Leone, A. Lombardi, K. L. Bren, Electrocatalytic CO_2 reduction by a cobalt porphyrin mini-enzyme, Chem. Sci. 16 (2025) 5707–5716, https://doi.org/10.1039/d4sc07026g.
[23] L. Leone, D. D'Alonzo, O. Maglio, V. Pavone, F. Nastri, A. Lombardi, Highly selective indole oxidation catalyzed by a mn-containing artificial mini-enzyme, ACS Catal. 11 (2021) 9407–9417, https://doi.org/10.1021/acscatal.1c01985.
[24] E. Renzi, A. Esposito, L. Leone, M. Chávez, T. Pineda, A. Lombardi, F. Nastri, Biohybrid materials comprising an artificial peroxidase and differently shaped gold nanoparticles, Nanoscale Adv. 6 (2024) 3533–3542, https://doi.org/10.1039/D4NA00344F.
[25] A. Esposito, L. Leone, A. De Simone, G. Fusco, F. Nastri, A. Lombardi, Catalytic nanomaterials by conjugation of an artificial heme-peroxidase to amyloid fibrils, ACS Appl. Mater. Interfaces 16 (2024) 45371–45382, https://doi.org/10.1021/acsami.4c10449.
[26] G. Zambrano, F. Nastri, V. Pavone, A. Lombardi, M. Chino, Use of an artificial miniaturized enzyme in hydrogen peroxide detection by chemiluminescence, Sensors 20 (2020) 3793, https://doi.org/10.3390/s20133793.
[27] E. Renzi, A. Piper, F. Nastri, A. Merkoçi, A. Lombardi, An artificial miniaturized peroxidase for signal amplification in lateral flow immunoassays, Small (2023) 2207949, https://doi.org/10.1002/smll.202207949.
[28] D. D'Alonzo, M. De Fenza, V. Pavone, A. Lombardi, F. Nastri, Selective oxidation of halophenols catalyzed by an artificial miniaturized peroxidase, Int. J. Mol. Sci. 24 (2023) 8058, https://doi.org/10.3390/ijms24098058.
[29] C. Mercier, P. Youmans, 4-Fluorophenol: A key intermediate for agrochemicals and pharmaceuticals, in: Industrial Chemistry Library, Elsevier, 1996, pp. 293–300, https://doi.org/10.1016/S0926-9614(96)80020-7.
[30] E.O. Igbinosa, E.E. Odjadjare, V.N. Chigor, I.H. Igbinosa, A.O. Emoghene, F. O. Ekhaise, N.O. Igiehon, O.G. Idemudia, Toxicological profile of chlorophenols and their derivatives in the environment: the public health perspective, Sci. World J. 2013 (2013) 460215, https://doi.org/10.1155/2013/460215.
[31] A. Sharma, L.A.B. Vázquez, E.O.M. Hernández, M.Y.M. Becerril, G. Oza, S.S.S. J. Ahmed, S. Ramalingam, H.M.N. Iqbal, Green remediation potential of immobilized oxidoreductases to treat halo-organic pollutants persist in wastewater and soil matrices - a way forward, Chemosphere 290 (2022) 133305, https://doi.org/10.1016/j.chemosphere.2021.133305.
[32] R. Pirzad, J.D. Newman, A.A. Dowman, D.C. Cowell, Horseradish peroxidase assay—radical inactivation or substrate inhibition? Revision of the catalytic sequence following mass spectral evidence, Analyst 119 (1994) 213–218, https://doi.org/10.1039/AN9941900213.
[33] R.L. Osborne, G.M. Raner, L.P. Hager, J.H. Dawson, C. *fumago* chloroperoxidase is also a dehaloperoxidase: oxidative dehalogenation of halophenols, J. Am. Chem. Soc. 128 (2006) 1036–1037, https://doi.org/10.1021/ja056213b.
[34] C.D. Murphy, Fluorophenol oxidation by a fungal chloroperoxidase, Biotechnol. Lett. 29 (2006) 45–49, https://doi.org/10.1007/s10529-006-9207-3.
[35] A.M. Osman, S. Boeren, C. Veeger, I.M.C.M. Rietjens, MP8-dependent oxidative dehalogenation: evidence for the direct formation of 1,4-benzoquinone from 4-fluorophenol by a peroxidase-type of reaction pathway, Chem. Biol. Interact. 104 (1997) 147–164, https://doi.org/10.1016/S0009-2797(97)00021-5.
[36] J. D'Antonio, E.L. D'Antonio, M.K. Thompson, E.F. Bowden, S. Franzen, T. Smirnova, R.A. Ghiladi, Spectroscopic and mechanistic investigations of dehaloperoxidase B from *amphitrite ornata*, Biochemistry 49 (2010) 6600–6616, https://doi.org/10.1021/bi100407v.
[37] M.K. Thompson, M.F. Davis, V. de Serrano, F.P. Nicoletti, B.D. Howes, G. Smulevich, S. Franzen, Internal binding of halogenated phenols in dehaloperoxidase-hemoglobin inhibits peroxidase function, Biophys. J. 99 (2010) 1586–1595, https://doi.org/10.1016/j.bpj.2010.05.041.
[38] G. Caserta, M. Chino, V. Firpo, G. Zambrano, L. Leone, D. D'Alonzo, F. Nastri, O. Maglio, V. Pavone, A. Lombardi, Enhancement of peroxidase activity in artificial Mimochrome VI catalysts through rational design, ChemBioChem 19 (2018) 1823–1826, https://doi.org/10.1002/cbic.201800200.
[39] L. Zoia, D.S. Argyropoulos, Phenoxy radical detection using ^{31} P NMR spin trapping, J. Phys. Org. Chem. 22 (2009) 1070–1077, https://doi.org/10.1002/poc.1561.
[40] L. Zoia, D.S. Argyropoulos, Detection of ketyl radicals using ^{31} P NMR spin trapping, J. Phys. Org. Chem. 23 (2010) 505–512, https://doi.org/10.1002/poc.1630.
[41] F. Sannino, P. Pernice, C. Imparato, A. Aronne, G. D'Errico, L. Minieri, M. Perfetti, D. Pirozzi, Hybrid TiO_2 –acetylacetonate amorphous gel-derived material with stably adsorbed superoxide radical active in oxidative degradation of organic pollutants, RSC Adv. 5 (2015) 93831–93839, https://doi.org/10.1039/C5RA21176J.
[42] V. Khramtsov, L.J. Berliner, T.L. Clanton, NMR spin trapping: detection of free radical reactions using a phosphorus-containing nitrone spin trap, Magn. Reson. Med. 42 (1999) 228–234, https://doi.org/10.1002/(SICI)1522-2594(199908)42:2<228::AID-MRM3>3.0.CO;2-T.
[43] C. Wang, L.L. Lovelace, S. Sun, J.H. Dawson, L. Lebioda, Complexes of dual-function hemoglobin/dehaloperoxidase with substrate 2,4,6-trichlorophenol are inhibitory and indicate binding of halophenol to compound I, Biochemistry 52 (2013) 6203–6210, https://doi.org/10.1021/bi400627w.
[44] B.E. Sturgeon, B.J. Battenburg, B.J. Lyon, S. Franzen, Revisiting the peroxidase oxidation of 2,4,6-trihalophenols: ESR detection of radical intermediates, Chem. Res. Toxicol. 24 (2011) 1862–1868, https://doi.org/10.1021/tx200215r.
[45] P. Ascenzi, M.G. Ascenzi, G. Amiconi, Enzyme competitive inhibition, graphical determination of Ki and presentation of data in comparative studies, Biochem. Educ. 15 (1987) 134–135, https://doi.org/10.1016/0307-4412(87)90043-4.
[46] M. Deodhar, S.B. Al Rihani, M.J. Arwood, L. Darakjian, P. Dow, J. Turgeon, V. Michaud, Mechanisms of CYP450 inhibition: understanding drug-drug interactions due to mechanism-based inhibition in clinical practice, Pharmaceutics 12 (2020) 846, https://doi.org/10.3390/pharmaceutics12090846.
[47] Y.-M. Kuo, R.A. Henry, A.J. Andrews, Measuring specificity in multi-substrate/product systems as a tool to investigate selectivity in vivo, Biochim. Biophys. Acta 1864 (2016) 70–76, https://doi.org/10.1016/j.bbapap.2015.08.011.
[48] J. Lind, X. Shen, T.E. Eriksen, G. Merenyi, The one-electron reduction potential of 4-substituted phenoxyl radicals in water, J. Am. Chem. Soc. 112 (1990) 479–482, https://doi.org/10.1021/ja00158a002.
[49] C. Li, M.Z. Hoffman, One-electron redox potentials of phenols in aqueous solution, J. Phys. Chem. B 103 (1999) 6653–6656, https://doi.org/10.1021/jp983819w.
[50] C. Liers, E. Aranda, E. Strittmatter, K. Piontek, D.A. Plattner, H. Zorn, R. Ullrich, M. Hofrichter, Phenol oxidation by DyP-type peroxidases in comparison to fungal and plant peroxidases, J. Mol. Catal. B Enzym. 103 (2014) 41–46, https://doi.org/10.1016/j.molcatb.2013.09.025.